ARTICLE

Check for updates

A synoptic bridge linking sea salt aerosol concentrations in East Antarctic snowfall to Australian rainfall

Danielle G. Udy [1,2,3✉], Tessa R. Vance [3], Anthony S. Kiem [4] & Neil J. Holbrook [1,2]

Previous research has shown that aerosol sea salt concentrations (Southern Ocean wind proxy) preserved in the Law Dome ice core (East Antarctica) correlate significantly with subtropical eastern Australian rainfall. However, physical mechanisms underpinning this connection have not been established. Here we use synoptic typing to show that an atmospheric bridge links East Antarctica to subtropical eastern Australia. Increased ice core sea salt concentrations and wetter conditions in eastern Australia are associated with a regional, asymmetric contraction of the mid-latitude westerlies. Decreased ice core sea salt concentrations and drier eastern Australia conditions are associated with an equatorward shift in the mid-latitude westerlies, suggesting greater broad-scale control of eastern Australia climate by southern hemisphere variability than previously assumed. This relationship explains double the rainfall variance compared to El Niño-Southern Oscillation during late spring-summer, highlighting the importance of the Law Dome ice core record as a 2000-year proxy of eastern Australia rainfall variability.

[1] Institute for Marine & Antarctic Studies, University of Tasmania, Hobart, TAS 7004, Australia. [2] ARC Centre of Excellence for Climate Extremes, University of Tasmania, Hobart, TAS 7004, Australia. [3] Australian Antarctic Program Partnership, Institute for Marine & Antarctic Studies, University of Tasmania, Hobart, TAS 7004, Australia. [4] Centre for Water, Climate and Land, College of Engineering, Science and Environment, University of Newcastle, Callaghan, NSW 2308, Australia. ✉email: danielle.udy@utas.edu.au

Subtropical climate regions experience highly variable rainfall and intense rainfall extremes. These regions also experience compound or sequential rainfall extremes that often result in shifts from persistent droughts to devastating floods[1–5] and extensive social, environmental and economic impacts[2,6,7]. Globally, the intensity and frequency of droughts and rainfall extremes are projected to increase due to anthropogenic climate change[8,9]. However, detecting the human influence on drought at regional scales is challenging, with clear climate change signals emerging in only selected regions (e.g., southwest Australia[10], western United States[11] and the Mediterranean[12]). In regions with substantial natural rainfall variability, such as eastern Australia, the background climate variability complicates the detection and attribution of human influence on recent droughts[8,9,13–15]. This uncertainty is largely due to relatively short instrumental-era rainfall records (~100 years), which likely misrepresents hydroclimate risk[16], in particular multidecadal 'megadroughts' known to have occurred throughout the past two millennia[17–20]. The short instrumental rainfall records also make it difficult to determine the underlying climate dynamics associated with the onset and termination of droughts and to evaluate if these processes are accurately represented in climate model simulations[21]. Millennial-scale rainfall proxies connected with the robust dynamical understanding of the mechanisms that underpin these palaeoclimate records provide critical information to estimate current and future rainfall variability and climate-related risks[20,22,23].

In contrast to the extensive palaeoclimate network across the Northern Hemisphere, Southern Hemisphere continents have limited spatial coverage of seasonal to annual resolution, continuous and long (>500 years) rainfall proxies[21,24]. Therefore, there is a need to explore remote climate proxies that have climatological links to Southern Hemisphere continents and preserve seasonal to annual signals of regional climate. One important example for eastern Australian rainfall is the Law Dome (LD) ice core (66°46′11″S,112°48′25″, elevation 1370 m), located on the East Antarctica coast[17,20,25]. LD's climate is predominantly maritime, with frequent incursions of Southern Ocean extratropical cyclones circulating around Antarctica[26]. This leads to LD receiving relatively uniform and high average annual snowfall (~1.5 m/year)[27], with occasional episodic snowfall events[28].

Austral summertime sea-salt aerosol concentrations from the LD ice core are significantly correlated to annual rainfall variability across eastern Australia[17,25]. Sea-salt aerosols preserved in the LD ice core record over austral summer represent an oceanic wind proxy of seasonal changes in the atmospheric circulation over the Indo-Pacific sector of the Southern Ocean[25,29]. Based on the relatively strong and significant correlation between LD summertime sea-salt (LD_{sss}) aerosol record and eastern Australian rainfall[17,25], and the clear alignment with dry and wet periods over eastern Australia seen in shorter local palaeoclimate records[24,30], the LD_{sss} record has been used to develop a 1000-year rainfall proxy for eastern Australian catchments[17,20,31,32]. This reconstruction highlights that recent droughts impacting eastern Australia (e.g., Millennium drought ~1997–2010) have not been unprecedented over the past 1000 years[17,20]. However, the dynamic mechanisms that underpin the statistical link between aerosol sea-salt deposits in East Antarctica and rainfall in eastern Australia have not been established. The efficacy and robustness of the relationship remain questionable without a clear mechanistic pathway between these climate regions. Here, we use synoptic weather typing[33] to define the dynamic relationship. We find that the sea-salt aerosol deposits at LD are associated with synoptic weather scale patterns that intermittently connect Southern Ocean wind strength and direction to rainfall processes across subtropical eastern Australia.

Results and discussion

Eastern Australian warm-season rainfall variability. Eastern Australian rainfall is highly variable due to interactions between the Pacific, Indian and Southern Oceans[1,34]. Tropical and extratropical modes characterising ocean and atmospheric variability, including El Niño-Southern Oscillation (ENSO)[35], the Southern Annular Mode (SAM)[36] and the Indian Ocean Dipole[37], interact to influence eastern Australia's rainfall[34]. However, these modes exhibit reduced influence during austral summer[34,38], especially over key agricultural regions in the Murray Darling Basin and drinking water catchments of major cities (e.g., Sydney and Brisbane; Fig. 1a and Supplementary Table 1) where summer rainfall is critical (i.e., >60% of annual rainfall is received between October and March)[39]. At the surface, easterly geostrophic winds are important for bringing moisture to subtropical eastern Australia from the Tasman and Coral Seas[40]. These conditions, in combination with orographic uplift over the Great Dividing Range[41] and favourable upper atmospheric circulation (i.e., ascending motion[42]), create suitable conditions for widespread rainfall and drought termination[38,43].

Austral warm-season teleconnection between Antarctica and Australia over the satellite era (1979–2016). The strongest connection between LD_{sss} and subtropical eastern Australian rainfall occurs during late austral spring–summer (Supplementary Table 1). Over late spring–summer (NDJF), the LD_{sss} record explains between 20 and 25% of the rainfall variance over the coastal eastern seaboard (ESB $r^2 = 0.21$, $P = 0.003$) and inland northern Murray Darling Basin (nMDB $r^2 = 0.25$, $P = 0.001$) regions. This relationship is stronger than either the influence of ENSO (Southern Oscillation Index[44]) or SAM (Marshall index[36]) on NDJF rainfall over nMDB ($ENSO_{NDJF}$ $r^2 = 0.13$, $P = 0.02$ | SAM_{NDJF} $r^2 = 0.04$, $P > 0.1$) and ESB ($ENSO_{NDJF}$ $r^2 = 0.14$, $P = 0.01$ | SAM_{NDJF} $r^2 = 0.03$, $P > 0.1$) (refer to Supplementary Table 2 for correlation results). In addition, the relationship between LD_{sss} and NDJF rainfall across nMDB ($r = +0.42$, $P < 0.01$, $n = 37$) and ESB ($r = +0.43$, $P < 0.01$, $n = 37$) is stronger than the relationship between ENSO and LD_{sss} ($r = +0.33$, $P < 0.05$, $n = 37$). This suggests that the teleconnection[17,25] is separate to, rather than a statistical artefact of, ENSO's influence on climate variability in both East Antarctica[45,46] and eastern Australia[34].

LD_{sss} is also strongly related to the summer (DJF) East Coast Flow Index[38] ($r = 0.50$, $P < 0.01$, $n = 37$), which describes both the surface and mid/upper-level atmospheric conditions (500hPa) required for summer rainfall over eastern Australia[40,42]. This suggests that atmospheric variability in the Indo-Pacific sector of the Southern Ocean is dynamically linked to favourable atmospheric processes required for summer rainfall across eastern Australia. We propose that LD_{sss} preserves the high-latitude influence on eastern Australian rainfall processes, particularly the mid/upper-level atmospheric conditions that either favour (ascending air) or inhibit (descending air) rainfall-promoting convection over eastern Australia. This is supported by regional rainfall distribution differences (Fig. 1b) and atmospheric composite conditions associated with years that have low (Fig. 1d; lower tercile <33%, $n = 12$) or high (Fig. 1e; upper tercile >66%, $n = 13$) sea-salt concentrations in summer (refer to Supplementary Fig. S1a for LD_{sss} timeseries split by tercile groups). The average late spring–summer rainfall over subtropical eastern Australia is significantly ($P < 0.05$) higher during high sea-salt years compared to low sea-salt years (Fig. 1b). The strongest signal is over the nMDB and ESB regions, where the average NDJF seasonal rainfall during high sea-salt years is 20% (~50 mm) and 14% (~70 mm) higher, respectively, than the average NDJF rainfall over the analysis period.
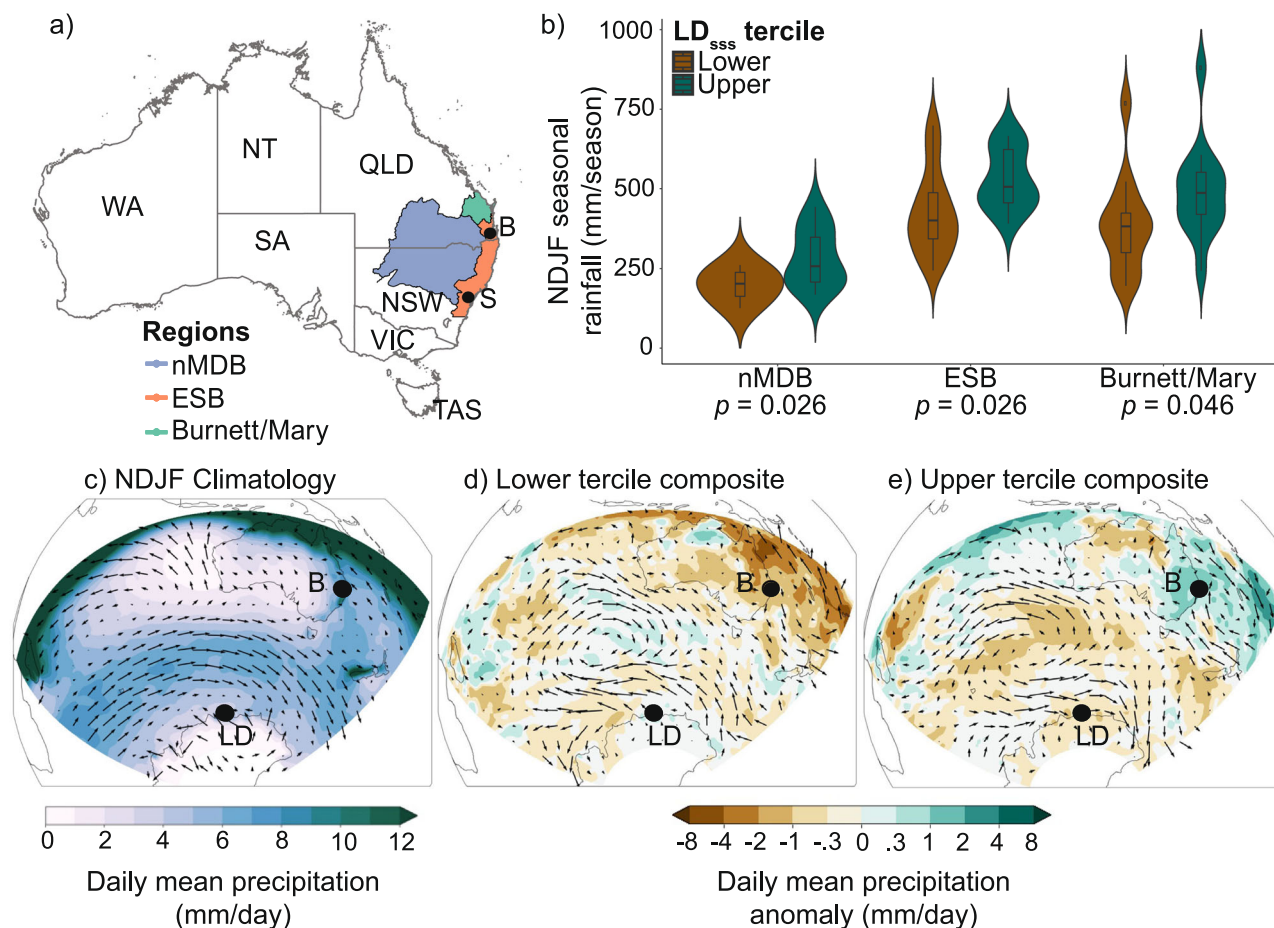
Fig. 1 Seasonal relationship between Law Dome summer sea salt (LD$_{sss}$) and eastern Australia rainfall over NDJF period from 1979/80 to 2015/16.
a Australia map including locations of major east coast cities of Brisbane (B) and Sydney (S) and rainfall regions most strongly correlated to LD$_{sss}$[17,25], incorporating key agricultural and urban water supply catchments; nMDB (blue) = northern Murray Darling Basin, ESB (orange) = eastern seaboard, and Burnett/Mary River catchment (green). **b** NDJF seasonal regional rainfall distributions over 1979/80 to 2015/16 for LD$_{sss}$ upper (LD$_{sss}$ > 0.192 logCl, $n = 13$) and lower (LD$_{sss}$ < 0.014 logCl, $n = 12$) tercile years (>66%, <33%). Wilcoxon signed-rank test used to determine the significance (95%) of mean regional rainfall between LD$_{sss}$ upper/lower tercile years over 1979/80–2015/16. Refer to Supplementary Fig. S1a for LD$_{sss}$ timeseries split by tercile groups. **c** NDJF climatology over 1979/80–2015/16 (ERA-Interim[58]) of daily total precipitation and surface winds (10 m) over study domain, including location of Brisbane (B) and Law Dome (LD). **d** NDJF composite conditions of daily total precipitation and surface wind (10 m) anomalies during LD$_{sss}$ lower tercile years. **e** As e during LD$_{sss}$ upper tercile years.

Identifying favourable synoptic conditions. We used a daily synoptic typing dataset constructed using self-organising maps, which we previously developed for the Indo-Pacific sector of the Southern Ocean[33], to investigate the synoptic conditions that link salt concentration of East Antarctic snowfall to eastern Australian rainfall ('Methods'). We hypothesised that the teleconnection between the two continents is due to synoptic weather patterns that cause strengthened (weakened) sea-salt aerosol generating westerly winds over the Southern Ocean off the LD coastline and moist onshore (dry offshore) winds over eastern Australia (Fig. 1d, e). This hypothesis is supported by the finding that average precipitation and surface wind anomalies identified in self-organised map three (SOM3: Fig. 2c) and seven (SOM7; Fig. 2g) characterise the synoptic conditions that would explain LD$_{sss}$ lower and upper tercile composite conditions respectively (Fig. 1d, e).

SOM3 is characterised by an equatorward shift in the mid-latitude westerlies leading to enhanced polar easterlies off the coastline of LD and dry offshore westerly winds over southern Australia (Fig. 2c), associated with negative rainfall anomalies over subtropical eastern Australia (Fig. 3c). This shift of the mid-latitude westerlies during late spring–summer is associated with descending air and reduced cloud cover[47], dynamically consistent

with the strong negative relationship between SOM3 and the East Coast Flow Index[38] ($r = -0.56$, $P < 0.001$, $n = 37$). In contrast, SOM7 is characterised by an asymmetric contraction of the mid-latitude westerlies and the co-occurrence of strengthened westerly winds over the Southern Ocean off the LD coastline, easterly winds over the Tasman/Coral Sea and an upper-level trough over south-eastern Australia[33] (Fig. 2g). The association with both surface easterly geostrophic flow and an upper-level trough is consistent with a strong positive correlation with the East Coast Flow Index ($r = +0.48$, $P < 0.01$, $n = 37$), inferring strong moist onshore flow and vertical ascent over eastern Australia[38]. These synoptic conditions are critical for widespread rainfall and drought termination across the Murray Darling Basin[38,40,43], and are associated with widespread positive rainfall anomalies across subtropical eastern Australia (Fig. 3g).

High-latitude synoptic processes associated with SOM3 and SOM7 are also preserved in the LD ice core, with a significant shift ($P < 0.01$) in average NDJF frequency of each synoptic type during LD$_{sss}$ lower and upper tercile years (Fig. 4c, g) and reduced (SOM3) or increased (SOM7) sea-salt aerosol production off the LD coastline (Fig. 5c, g). Increased frequency of SOM3 is related to low LD$_{sss}$ concentrations ($r_{NDJF} = -0.46$, $P < 0.01$,
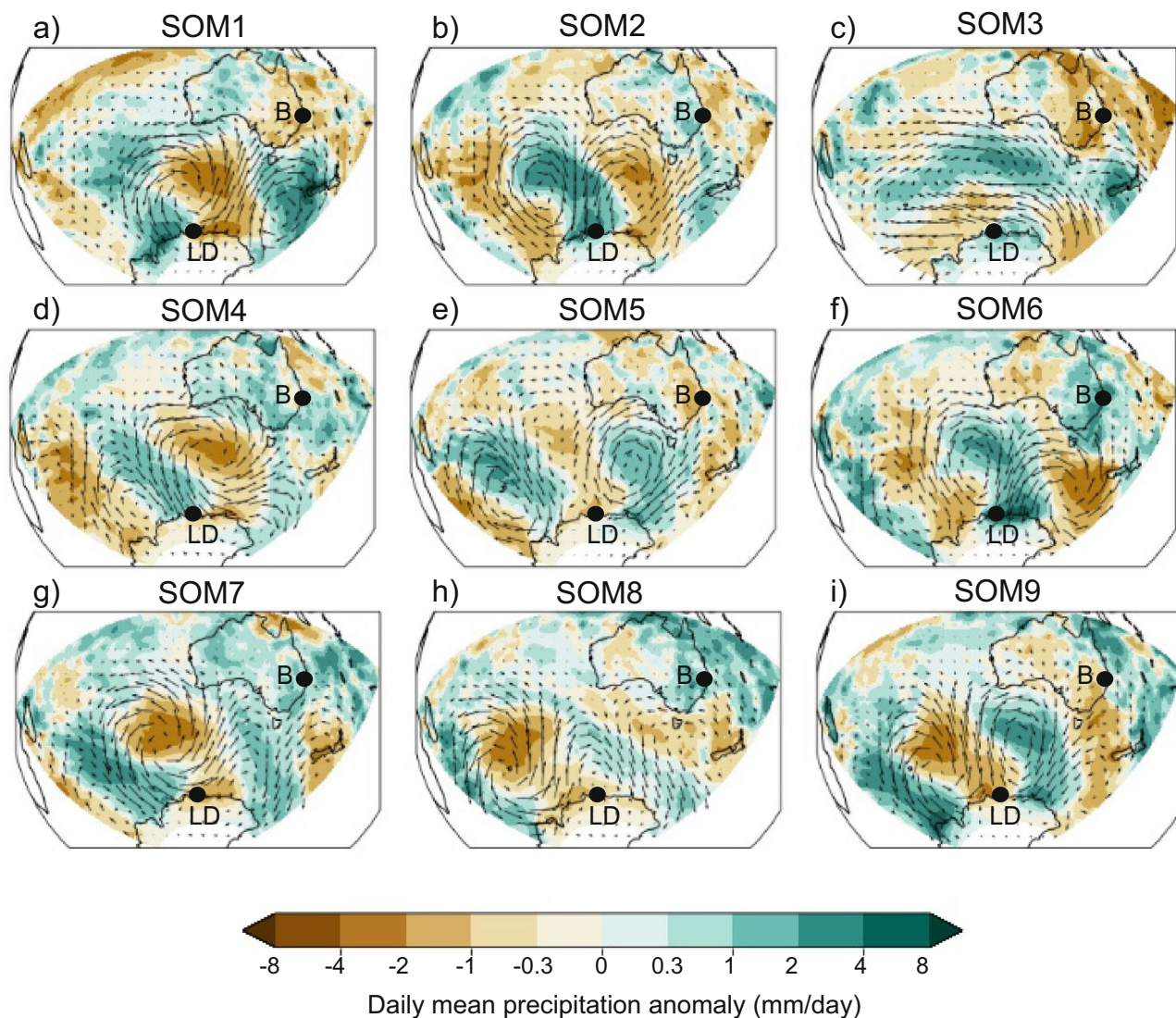
Fig. 2 NDJF daily total precipitation and surface (10 m) wind anomaly (data: ERA-Interim[58]) for the nine SOM nodes from ref. [33] over 1979/80 to 2017/18. SOM nodes 1 to 9 are labelled (**a–i**). SOM composite anomalies calculated from the NDJF climatology (Fig. 1c). SOM3 (SOM7) supports lower (upper) LD_{sss} composite conditions (Fig. 1d, e), reflecting reduced (strengthened) westerly winds near Law Dome (LD) coastline and dry (wet) eastern Australia (B = Brisbane). Note the precipitation scale is non-linear.

$n = 37$), and increased SOM7 frequency corresponds with high LD_{sss} concentrations ($r_{NDJF} = +0.47$, $P < 0.01$, $n = 37$). Other synoptic types are associated with either widespread rainfall conditions over eastern Australia (SOM6; Fig. 2f) or increased westerly winds near LD (SOM4, Fig. 2d), but the corresponding conditions over LD or eastern Australia respectively do not support the teleconnection. SOM6 is associated with widespread rainfall over eastern Australia (Fig. 3f), consistent with Tasman Sea blocking[33,34]. However, we found no relationship between SOM6 and LD_{sss} (Supplementary Table 1), or any significant shift in distribution between high and low sea-salt concentration years (Fig. 4f). Nevertheless, SOM6 was found to be associated with strong positive precipitation anomalies (+8 mm/day) over LD (Fig. 2f). This is reflected in the ice core record with high snowfall accumulation years significantly related to the increased annual frequency of SOM6 ($r = +0.44$, $P < 0.01$, $n = 37$). Importantly, this highlights that the observed teleconnection to eastern Australian rainfall is based on the aerosol salt loading of the snowfall deposited at LD, rather than the amount of snowfall.

We also found the NDJF frequency of SOM4 to be significantly correlated with LD_{sss} ($r = +0.42$, $P < 0.01$, $n = 37$), and a significant ($P < 0.05$) distribution shift between high- and low sea-salt concentration years (Fig. 4d). However, the region of influence on eastern Australia rainfall is focused further south than the LD_{sss} correlation region[17,25] (Fig. 3d).

Synoptic bridge linking Antarctic ice core record to Australian rainfall. The synoptic pattern over the Indo-Pacific sector of the Southern Ocean required to support both increased sea-salt concentrations at LD, and favourable convection conditions over eastern Australia (Fig. 6a) consists of:

- Two surface high-pressure systems to the southwest and southeast of Australia, centred over the south-eastern Indian Ocean and New Zealand, respectively, and
- A surface cold front approaching Tasmania, in between the two high-pressure systems, with a mid/upper-level trough extending equatorward over south-eastern Australia.
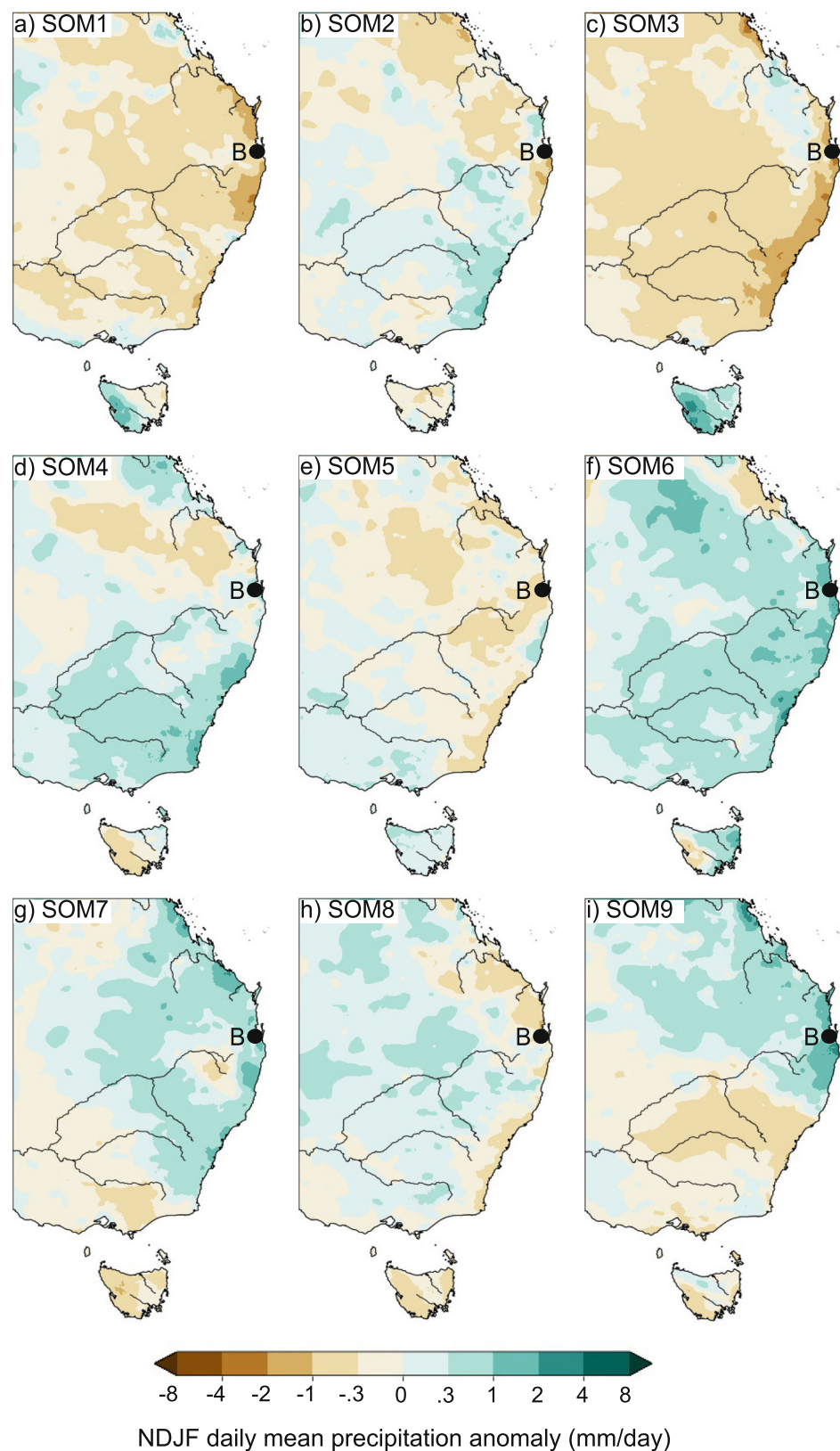
Fig. 3 NDJF daily mean rainfall anomaly (dataset: AGCD v1[65]) over eastern Australia for each SOM node from ref. [33] over 1979/80 to 2017/18. SOM nodes 1 to 9 are labelled (**a**–**i**). B = Brisbane. Note the precipitation scale is non-linear.
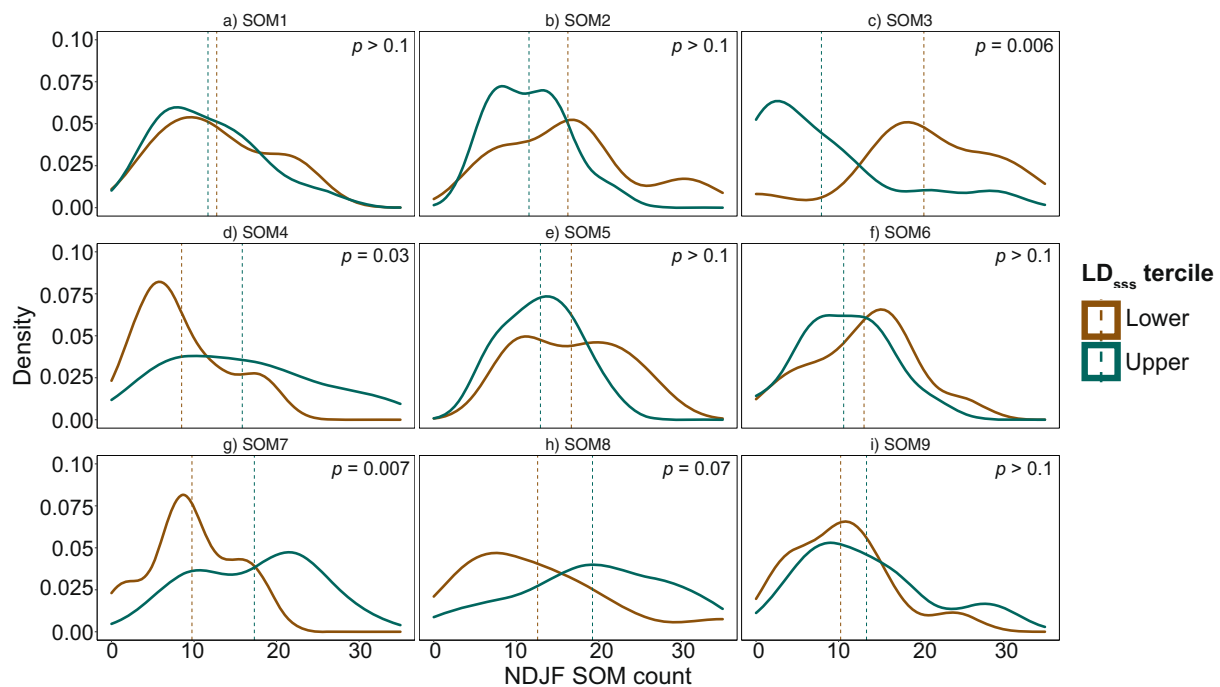
Fig. 4 Probably density curves of NDJF SOM frequency for Law Dome summertime sea-salt (LD$_{sss}$) concentration upper ($n = 13$) and lower ($n = 12$) tercile years and mean frequency of each group (dashed vertical line) for each SOM node in ref. [33]. SOM nodes 1 to 9 are labelled (**a–i**). The Wilcoxon signed-rank test was used to test if there was a significant difference (90%) between the mean frequency of upper/lower tercile years for each SOM node ($P < 0.1$ for SOM3, SOM4, SOM7 and SOM8).

The south-eastern Indian Ocean high-pressure system is associated with a ridge that extends towards East Antarctica, resulting in an asymmetric poleward contraction of the mid-latitude westerlies towards the LD coastline. The extratropical cyclones embedded in the westerlies provide favourable conditions for increased sea-salt from ocean-derived aerosols generated upstream from the ice core site, as well as a mechanism for transport and deposition of the sea-salt aerosols in snowfall across LD[26,29] (Fig. 5g). Importantly, while SOM7 is associated with below-average precipitation over LD (Fig. 2g), it does not necessarily mean that no snowfall occurs. The majority of snowfall at LD is associated with either orographic snowfall from strengthened polar easterlies (SOM3; Fig. 2c) or extreme episodic snowfall events with mid-latitude interaction[28,46,48] (SOM2 and SOM6; Fig. 2b, f).

For eastern Australia, the combination of surface high pressure over New Zealand with a ridge extending towards Australia and a mid/upper-level trough over southeast Australia provide favourable rainfall conditions (Fig. 3g), through moisture advection from the Coral/Tasman Sea[40,43] and ascending air motion respectively[38,42]. In addition, the synoptic set-up near the southwestern Australian coastline supports the positive rainfall correlation identified in ref. [17], with onshore coastal showers associated with the eastern flank of the Indian Ocean high-pressure system (Fig. 2f).

During austral spring–summer, these synoptic patterns are more likely during La Niña and positive SAM climatic conditions[33]. The connection to La Niña is consistent with previous research both for LD and eastern Australia, with La Niña associated with increased LD$_{sss}$[25,49] and above average spring–summer rainfall over eastern Australia[34,50]. Although positive SAM is linked to increased rainfall over eastern Australia during spring[34], the LD$_{sss}$ record has not been previously found to have a strong relationship with SAM[25,45,49]. The weak SAM signal in the LD$_{sss}$ record can be explained by a combination of a

one-month shift in atmospheric conditions compared to the ice core 'months' (i.e., atmosphere NDJF, ice core DJFM; see 'Methods') and multiple synoptic arrangements of positive SAM conditions[33]. SAM variability over NDJF is significantly related to LD$_{sss}$ (1979/80–2015/16: $r = +0.48$, $P < 0.01$), but drops below 95% significance over DJFM[25,49]. Due to the asymmetry in the contraction of the mid-latitude westerlies during positive SAM conditions[33], only part of the positive SAM signal is captured by increased LD$_{sss}$. The sea-salt signal associated with SOM8 is weak at LD due to the westerlies arcing away from the LD coastline (Figs. 4h and 5h). This complicates the SAM signal in the LD$_{sss}$ record, as positive SAM seasons dominated by SOM8 will have lower sea-salt concentrations compared to positive SAM seasons dominated by SOM7. This is important to consider for the teleconnection to eastern Australia, as SOM8 is also associated with positive rainfall anomalies over inland regions (Fig. 3h). However, the signal is not as widespread or as strong as SOM7. For NDJF, SOM8 frequency explains 5% of the nMDB rainfall variability compared to 20% for SOM7.

Low sea-salt concentrations in LD summer snowfall are typically associated with an equatorward shift of the subtropical ridge over southern Australia and extratropical cyclones/cold fronts in the Southern Ocean (Fig. 6b). These conditions result in polar easterlies and reduced aerosol sea-salt production (Fig. 5c) near the LD coastline[45], and low rainfall (Fig. 3c) due to convection-inhibiting conditions over eastern Australia during late spring–summer[47]. They are also associated with an increased likelihood of eastern Australian heatwaves, bushfires, and severe drought conditions in late spring-early summer[47,51]. These synoptic conditions are more likely during negative SAM[33], and seasons dominated by SOM3 correspond with reduced frequency of SOM7 ($r = -0.45$, $P < 0.01$, $n = 37$).

Recommendations for using the LD$_{sss}$ record in eastern Australian rainfall reconstructions. The synoptic connection identified
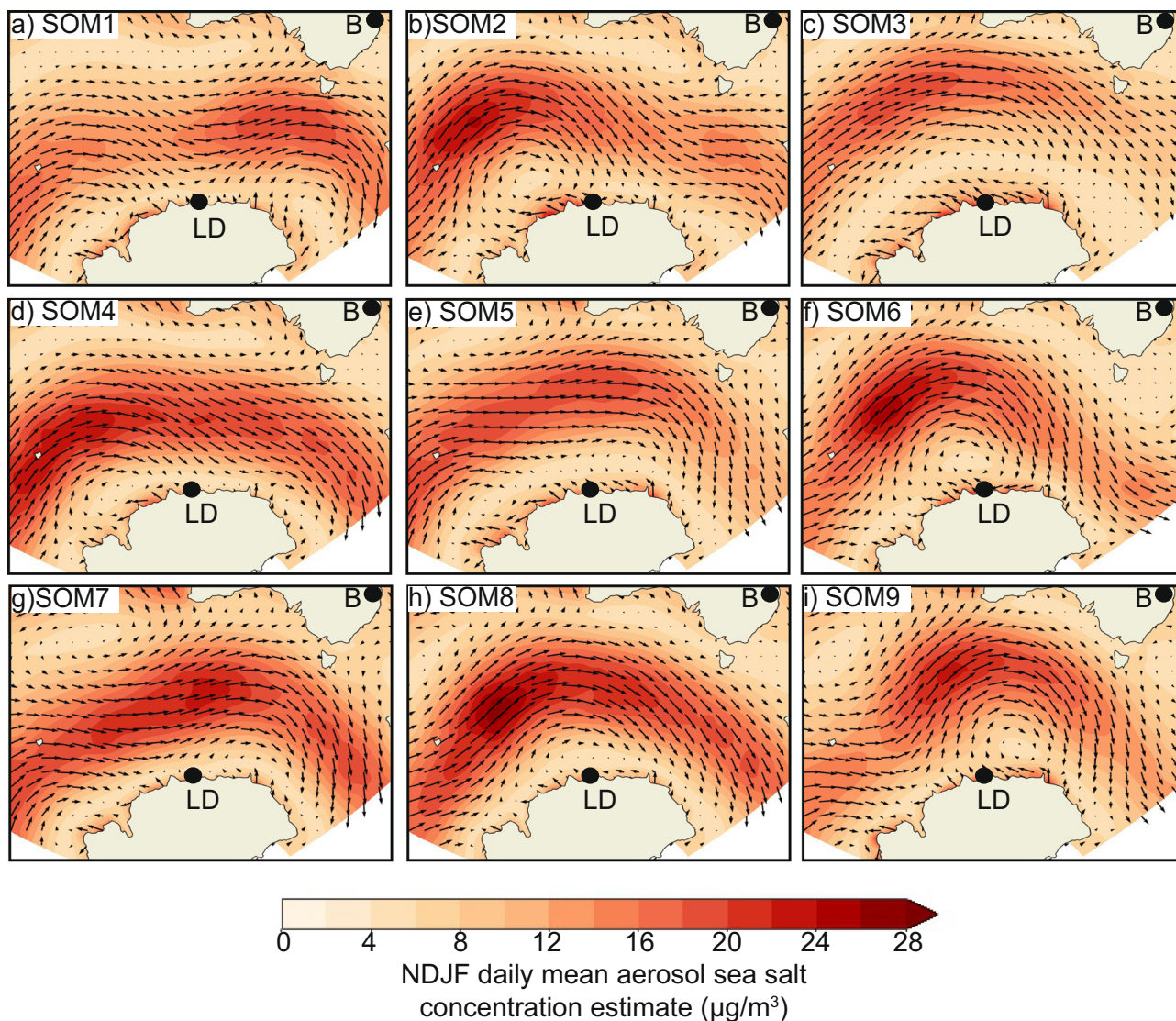
Fig. 5 NDJF estimated daily mean sea-salt aerosol generation* and mean surface (10 m) wind conditions (data: ERA-Interim[58]) for each SOM node from ref. [33]. SOM nodes 1 to 9 are labelled (**a–i**). B = Brisbane, LD = Law Dome. *Sea-salt aerosol generation is estimated at each grid point using the ref. [64] equation, which relates sea-salt aerosol generation to local surface wind speed.

between LD and subtropical eastern Australia provides confidence in using the remote LD_{sss} proxy record to assist with identifying the frequency and duration of wet and dry periods in eastern Australia to inform water policy and infrastructure decisions. As the direct synoptic connection occurs over late spring–summer (NDJF), it is recommended that warm-season rainfall variability be the focus when using LD_{sss} as an input for rainfall reconstructions over the past millennia. Nevertheless, if the majority of the annual rainfall occurs during the warm season, continued use of the LD_{sss} record t`o inform annual (water year) rainfall variability may also be appropriate[20].

Combining the LD_{sss} record, which reflects part of the Southern Ocean/Antarctic influence on eastern Australian rainfall, with other proxy records that capture variability in the Pacific and Indian Oceans would likely result in an increased rainfall variance explained and benefit the water resource sector. However, prior to incorporating the LD_{sss} record into future multi-proxy reconstructions, we recommend that the seasonal synoptic weather connection between multi-proxy locations and the target region be considered to ensure the dynamic relationships are maintained.

As the LD_{sss} record is a seasonal signal, we expect the connection to eastern Australian rainfall to be strongest during years when either frequent rainfall occurs throughout the entire late spring–summer season (e.g., 2007/08 and 2010/11) or limited rainfall occurs throughout the season (e.g., 1982/83 and 1986/87), and weaken or collapse when seasonal rainfall is dominated by an extreme event (e.g., 2012/13). The strongest connection seasons frequently align with strong ENSO and SAM events being in phase, with La Niña/positive SAM NDJF seasons (e.g., 2007/08 and 2010/11) generally strengthening the high sea-salt and high rainfall connection (Supplementary Fig. 1). Interestingly, in NDJF seasons when El Niño/negative SAM are in phase the connection is maintained, but not necessarily with low sea salt and low rainfall which would be expected based on El Niño and/or negative SAM conditions during late spring–summer. For example, NDJF seasons of 1982/83, 1986/87, 1991/92 and 2009/10 are characterised as El Niño and negative SAM but only 1982/83 and 1986/87 recorded low sea salt and below-average rainfall. The NDJF seasons of 1991/92 and 2009/10 recorded high sea salt and average or above average rainfall despite El Niño and negative SAM conditions, highlighting the additional rainfall
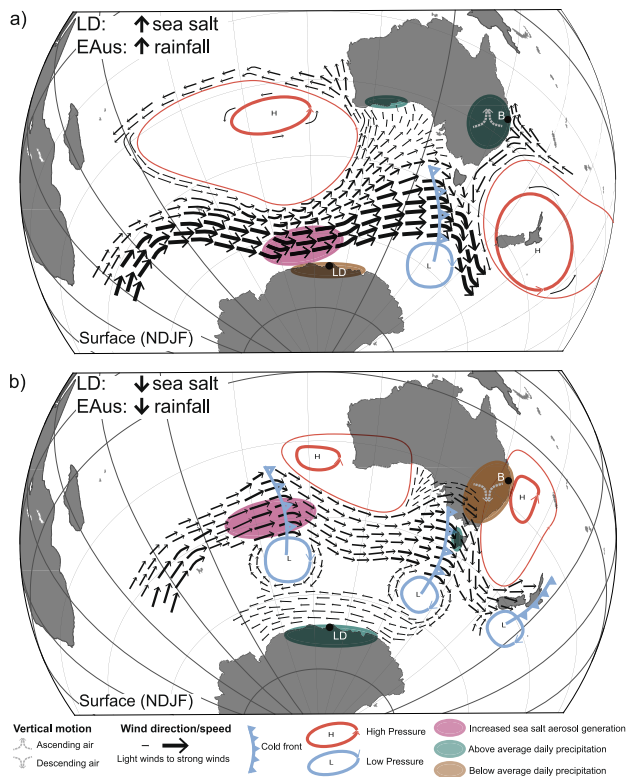
Fig. 6 Schematic of favourable synoptic weather conditions (late austral spring–summer) in the Indo-Pacific sector of the Southern Ocean that support the observed teleconnection between Law Dome summer sea-salt (LD$_{sss}$) and subtropical eastern Australia rainfall. a Increased LD$_{sss}$ linked to above average rainfall in eastern Australia. **b** Decreased LD$_{sss}$ linked to below-average rainfall in eastern Australia.

variance explained by the LD$_{sss}$ record compared to ENSO or SAM in austral spring–summer across subtropical eastern Australia. The focus of El Niño anomalies—either central Pacific or eastern Pacific[52]—may contribute to some of this discrepancy, with central Pacific El Niño events linked with increased rainfall across the Murray Darling Basin over late spring–summer[53]. In addition, the strongest sea surface temperature anomalies associated with the central Pacific El Niño event in 2009/10 were in the extratropical south-central Pacific rather than the tropics, changing the influence on the mid-latitude westerly wind belt and Antarctic climate[54].

The 2012/13 season is an example of when the connection collapses, with low sea-salt concentrations in Law Dome snowfall but above average rainfall for eastern Australia (Supplementary Fig. 1). This season would have been characterised as below-average rainfall across eastern Australia except for four days of extreme rainfall (>99.5th percentile daily rainfall) associated with ex-Tropical Cyclone Oswald in late January and an east coast low in late February (e.g., seasonal rainfall total for ESB region in 2012/13 including all days = 699 mm vs 427 mm with 4 extreme rain days removed). This example of an event-scale signal (extreme rainfall) that contrasts with the seasonal-scale signal (below-average rainfall during the remainder of the season and low sea-salt aerosol concentrations) is unlikely to be resolved by the ice core record, which can only record the dominant seasonal-scale conditions. If extreme rainfall days (>99.5th percentile) are removed from the seasonal total, the variance explained by the LD$_{sss}$ record in the ESB region increases from 21 to 33% over the 1979/80 to 2015/16 period. Nonetheless, we have not removed

these extremes, as it is important to represent the variance explained over the full record, including extreme rainfall events.

Conclusions. In summary, aerosol sea-salt concentrations in summer snowfall deposited at LD preserve the high-latitude synoptic influence on austral warm-season rainfall variations across subtropical eastern Australia. The observed teleconnection between high LD$_{sss}$ concentrations and increased rainfall over eastern Australia is dynamically supported by surface and mid/upper-level atmospheric conditions that promote warm-season convection over eastern Australia, corresponding with an asymmetric contraction of the mid-latitude westerlies toward LD. These late spring–summer periods are often associated with consecutive widespread rainfall events across eastern Australia, increasing the likelihood of drought termination and floods. In contrast, periods of low LD$_{sss}$ concentrations and decreased rainfall across eastern Australia are characterised by an equatorward shift in the mid-latitude westerlies. These conditions inhibit warm-season convection over eastern Australia, increasing the possibility of drought initiation or persistence.

The combination of a synoptic bridge linking East Antarctica and Australia, and the annually resolved multi-centennial ice core record (2000 + years[55]) provides an opportunity for a dynamically based rainfall reconstruction that massively extends the ~100 yr instrumental rainfall record in eastern Australia. This enables us to derive a long-term baseline of plausible hydroclimate extremes to (i) assist in the detection of human influence on recent droughts; (ii) use in hydroclimate risk quantification (e.g., inform planning/strategies aimed at ensuring water/food/energy security) and (iii) evaluate the representation of dynamic rainfall processes in historical climate model simulations to help reduce uncertainties associated with regional rainfall projections. Furthermore, this research creates possibilities for other subtropical climate records for the Southern Hemisphere being derived from existing and new East Antarctic ice cores (e.g., LD; Mount Brown South[49,56]) to be used to match the hydroclimate baseline understanding gained from vast tree-ring networks in the Northern Hemisphere[11].

Methods

Study domain. The study domain outlined in ref. [33] was extended equatorward in this study to investigate teleconnections between East Antarctica and eastern Australia (10–75°S, 40–180°E). Here, eastern Australia has been divided into three regions (Fig. 1a) that fall within the strongest correlation region of LD$_{sss}$ to annual rainfall[17,25]:

1. Inland agricultural region of the northern Murray Darling Basin (nMDB) which incorporates the Barwon–Darling catchment upstream of Menindee Lakes;
2. Eastern Seaboard (ESB) incorporating the coastal region east of the Great Dividing Range from 25°S to 35°S and including major cities and water supply catchments of Brisbane and Sydney; and
3. Coastal agricultural region of the Burnett/Mary River catchment, north of Brisbane.

Synoptic typing dataset. The daily synoptic typing dataset[57] for the southern Indian Ocean from ref. [33] was used to classify the dominant large-scale weather patterns of each day from January 1979 to October 2018 into nine synoptic types. This dataset was created using a self-organising maps (SOMs) algorithm on 500 hPa geopotential height daily anomalies from ERA-Interim reanalysis data[58]. The combination of nine (3 × 3) nodes was selected based on visual inspection, a performance score of the SOMs, and discussions with meteorologists working in the study region[33].

Synoptic classification relies on the assumption that atmospheric patterns can be partitioned into a specific number of 'types'. For this reason, the SOM algorithm is often preferred over traditional clustering methods (e.g., k-means) to classify weather patterns, as it can account for both the continuity and non-linearity of weather[59]. The SOM algorithm achieves this by categorising data more uniformly, preserving the probability density of the input data, as well as maintaining the topological order of the data by updating both the 'winning' node and neighbourhood nodes at each iteration[60]. SOMs have been successfully used to

analyse synoptic weather patterns in the Southern Ocean[1,61] and have contributed to improved interpretation of West Antarctic ice core climate proxies[62].

Climate indices. The DJF seasonal East Coast Flow Index (ECFI)[38] provided an estimate of the combined influence of easterly surface geostrophic winds along eastern Australia and vertical ascent, both important for creating favourable widespread rainfall conditions. The ECFI combines the influence of ENSO and SAM over subtropical eastern Australia and provides a physical link between the large-scale forcing and local precipitation response[38]. High positive values indicate strong onshore flow and vertical ascent over the ESB, resulting in a moist environment that is favourable for convection[38].

We also used the monthly Marshall index[36] to determine the phase of SAM, the Dipole Mode Index (DMI) for the Indian Ocean Dipole[37], and a combination of the atmospheric sea-level pressure (Southern Oscillation Index)[44] and sea surface temperature anomaly (SSTA) indices (Oceanic Niño Index (ONI): 3-month running mean of SSTA in the Niño3.4 region)[63] to represent the phase of ENSO.

Gridded climate data. To explore surface weather conditions across the entire study domain associated with each SOM node defined in ref. [33], we used the 'total precipitation', and surface (10 m) 'u' and 'v' wind variables from ERA-Interim. These variables were chosen as they influence the snowfall accumulation and sea-salt aerosol concentration (Southern Ocean wind proxy) records in the ice core. Although ERA5 is now available and offers higher resolution, ERA-Interim was used to be consistent with the reanalysis model used for defining the synoptic types[33]. For each variable investigated, the annual and seasonal anomalies for each synoptic type were calculated by subtracting the climatological mean over the SOM analysis period (1979–2018) from the mean conditions of each SOM node. Analysis was undertaken for all seasons, plus alternative four monthly seasons over austral spring–summer (ONDJ, NDJF and DJFM). We focus on seasonal results for NDJF in the main text.

Estimating sea-salt aerosol generation over the Southern Ocean. An estimate of potential sea-salt aerosol generation at each grid point in the study domain for each SOM node was calculated from mean wind speed using the ref. [64] equation, where 'C' is potential sea salt aerosol generation ($\mu g/m^3$) and 's' is the local surface wind speed:

$$C = \exp{(0.16s + 1.45)}$$

Eastern Australia daily rainfall observations. Daily rainfall observations over eastern Australia were sourced from the Australian Gridded Climate Data (AGCD) v1 (previously Australian Water Availability Project; AWAP)[65]. The AGCD v1 dataset provides daily gridded rainfall fields extending back to 1900 on a $0.05° \times 0.05°$ grid and is widely used for studying rainfall variability over eastern Australia. AGCD v1 data were used to calculate SOM rainfall anomalies for each grid point over eastern Australia, and area average rainfall for nMDB, ESB and the Burnett/Mary River catchment regions.

Law Dome ice core data. We used two Law Dome (LD) ice core proxy records, Law Dome summertime sea-salt concentrations (LD_{sss}) and annual snowfall accumulation, to determine if synoptic weather patterns can be preserved in the ice core record at a seasonal (austral summer) or annual scale, respectively[25,27,49,55,66]. The ice core site (Dome Summit South: DSS) receives a high annual snowfall of 0.68 m ice equivalent/year (~1.5 m of snowfall)[27] which produces seasonally varying annual layers in the ice core and corresponds to annual and seasonal climate signals[25,67,68]. The DSS ice core record is primarily dated using seasonally varying water stable isotopes ($\delta^{18}O$ and δD) which peak in austral summer (10th January average)[69]. These annually resolved and accurately dated layers (+/−0 years over 1815–2016)[70] make the LD record useful for hydroclimate studies where accurate event timing, duration, and high sample temporal resolution (seasonal–annual) are required[20]. The DSS record used in this study combines two overlapping ice cores (DSS1617 and DSS97)[49] to span the period of the synoptic typing dataset (1979–2016). The DSS1617 portion of the record (drilled in the austral summer 2016/17) extends the upper portion of the DSS record presented in ref. [25] and covers the period 1989–2016. The DSS97 core covers the period 1888–1989, but for the purposes of this study is used from 1979. The LD sea-salt record is derived from trace chemical analysis (liquid ion chromatography)[49] of discrete 5 cm samples yielding a sample resolution averaging 21 samples y^{-1} between 1950 and 2016 (~22 samples/year over 1979–2016). Assuming seasonally uniform annual snowfall, the chloride record is split into 12 estimated monthly bins. The LD_{sss} record is calculated by averaging the ice core estimated 'December to March' (DJFM) period chloride log transformed[25] concentrations (~7 samples/year). While Law Dome receives frequent snowfall, the accumulation is not completely uniform. Thus, the ice core 'DJFM' period approximates the austral summer period but may not directly align with DJFM atmospheric conditions.

At coastal ice core sites, sea-salt aerosol scavenging is dominated by wet deposition[71]. Therefore, net accumulation is required at LD for both annual accumulation and LD_{sss} records to capture any climate signal. ERA-Interim

captures both the temporal accumulation variability ($r = 0.69$, $P < 0.001$; 1979–2013) and average annual snowfall accumulation rate (ERA-Interim: 0.713 +/− 0.136 metres ice equivalent/year vs DSS ice core: 0.749 +/− 0.142 metres ice equivalent/year)[27,49]. This provides confidence that ERA-Interim can be usefully used to investigate surface condition anomalies associated with the synoptic types and how they are potentially preserved in the LD record. It is also important to recognise the ice core record limitations, with conditions such as snowfall hiatus (i.e., periods of no snowfall) or surface redistribution (i.e., snow being blown away) potentially disrupting or masking signal preservation and dating accuracy. Over the satellite era, this is minimal at Law Dome with snowfall occurring in all summer periods (i.e., no missed years; Supplementary Fig. 2), and minimal surface redistribution due to katabatic winds diverting around the dome[56,72].

Linking coastal sea-salt concentrations in the snow in East Antarctica to eastern Australia rainfall. Timeseries analysis using Spearman/Pearson correlations was used to explore relationships between the synoptic-type seasonal/annual frequency, ice core trace chemistry and accumulation records (LD_{sss}, annual accumulation), climate modes of variability (ECFI, ENSO, IOD and SAM) and eastern Australian rainfall (area averaged to nMDB, ESB and Burnett/Mary River catchment). Focusing on the austral warm season, the analysis was carried out for a combination of three- and four-month seasons from October to March (OND to JFM and ONDJ to DJFM). Prior to the correlation analysis, annual (Jan-Dec) and seasonal (as above) SOM frequency timeseries were calculated for each SOM node by counting each daily occurrence within a year (for comparison to annual accumulation) or warm-season period (for comparison to LD_{sss}). All timeseries were detrended and tested for autocorrelation and normality. No significant autocorrelation was detected. However, the seasonal synoptic-type frequency timeseries were often positively skewed. The Spearman correlation method was used for all seasonal correlations (e.g., $SOM1_{seasonal} \sim LD_{sss}$) and the Pearson method was used for annual correlations (e.g., $SOM1_{annual} \sim DSS$ annual accumulation). The two-sided Student's t test analysed against significance at the 95% confidence level was used to test the significance of an observed correlation score. The LD_{sss} record was also split into the upper ($n = 13$) and lower ($n = 12$) tercile years for the period 1979–2016 to explore frequency distribution and mean changes in the synoptic types, and area average rainfall between high and low summer sea-salt years (Supplementary Fig. S1a). The Wilcoxon signed-rank test was used to determine if the mean difference between the two groups was statistically significant at the 90% level. The 90% level was selected as the limited number of observations over the satellite era in each group ($n = 12$) influenced the power of the Wilcoxon signed-rank test.

Data availability

Code availability

All the scripts (mix of python and R) utilised for our analysis are available by contacting the corresponding author.

References

1. Verdon-Kidd, D. C. & Kiem, A. S. On the relationship between large-scale climate modes and regional synoptic patterns that drive Victorian rainfall. *Hydrol. Earth Syst. Sci.* **13**, 467–479 (2009).

2. van Dijk, A. I. J. M. et al. The Millennium Drought in southeast Australia (2001–2009): Natural and human causes and implications for water resources, ecosystems, economy, and society. *Water Resour. Res.* **49**, 1040–1057 (2013).

3. Kiem, A. S. et al. Natural hazards in Australia: droughts. *Clim. Change* **139**, 37–54 (2016).

4. Johnson, F. et al. Natural hazards in Australia: floods. *Clim. Change* **139**, 21–35 (2016).

5. Baek, S. H., Smerdon, J. E., Cook, B. I. & Williams, A. P. U. S. Pacific coastal droughts are predominantly driven by internal atmospheric variability. *J. Clim.* **34**, 1947–1962 (2021).

6. De Kauwe, M. G. et al. Identifying areas at risk of drought-induced tree mortality across South-Eastern Australia. *Glob. Change Biol.* **26**, 5716–5733 (2020).

7. Lund, J., Medellin-Azuara, J., Durand, J. & Stone, K. Lessons from California's 2012-2016 Drought. *J. Water Resour. Planning Manag.* **144**, 04018067 (2018).

8. Seneviratne, S. I. et al. Weather and Climate Extreme Events in a Changing Climate. In *Climate Change 2021: The Physical Science Basis. Contribution of Working Group I to the Sixth Assessment Report of the Intergovernmental Panel on Climate Change.* (eds. Masson-Delmotte, V. et al.) pp. 1513–1766 (Cambridge University Press, Cambridge, United Kingdom and New York, NY, USA, 2021).

9. Douville, H. et al. Water Cycle Changes. In *Climate Change 2021: The Physical Science Basis. Contribution of Working Group I to the Sixth Assessment Report of the Intergovernmental Panel on Climate Change.* (eds. Masson-Delmotte, V. et al.) pp. 1055–1210 (Cambridge University Press, Cambridge, United Kingdom and New York, NY, USA, 2021).

10. Delworth, T. L. & Zeng, F. Regional rainfall decline in Australia attributed to anthropogenic greenhouse gases and ozone levels. *Nat. Geosci.* **7**, 583–587 (2014).

11. Williams, A. P. et al. Large contribution from anthropogenic warming to an emerging North American megadrought. *Science* **368**, 314–318 (2020).

12. Marvel, K. et al. Twentieth-century hydroclimate changes consistent with human influence. *Nature* **569**, 59–65 (2019).

13. Kirono, D. G. C., Round, V., Heady, C., Chiew, F. H. S. & Osbrough, S. Drought projections for Australia: updated results and analysis of model simulations. *Weather Clim. Extremes* **30**, 100280 (2020).

14. Dowdy, A. G. et al. Rainfall in Australia's eastern seaboard: a review of confidence in projections based on observations and physical processes. *Australian Meteorol. Oceanographic J.* **65**, 107–126 (2015).

15. Dey, R., Lewis, S. C., Arblaster, J. M. & Abram, N. J. A review of past and projected changes in Australia's rainfall. *WIREs Clim. Change* **10**, e577 (2019).

16. Vance, T. R. et al. Pacific decadal variability over the last 2000 years and implications for climatic risk. *Commun. Earth Environ.* **3**, 33 (2022).

17. Vance, T. R., Roberts, J. L., Plummer, C. T., Kiem, A. S. & van Ommen, T. D. Interdecadal Pacific variability and eastern Australian megadroughts over the last millennium. *Geophysical Res. Lett.* **42**, 129–137 (2015).

18. Cook, E. R. et al. Megadroughts in North America: placing IPCC projections of hydroclimatic change in a long-term palaeoclimate context. *J. Quatern. Science.* **25**, 48–61 (2010).

19. Cook, B. I. et al. North American megadroughts in the Common Era: reconstructions and simulations. *WIREs Clim. Change* **7**, 411–432 (2016).

20. Kiem, A. S. et al. Learning from the past—using palaeoclimate data to better understand and manage drought in South East Queensland (SEQ), Australia. *J. Hydrol.: Regional Studies* **29**, 100686 (2020).

21. Steiger, N. J., Smerdon, J. E., Cook, E. R. & Cook, B. I. A reconstruction of global hydroclimate and dynamical variables over the Common Era. *Sci. Data* **5**, 180086 (2018).

22. Armstrong, M. S., Kiem, A. S. & Vance, T. R. Comparing instrumental, palaeoclimate, and projected rainfall data: Implications for water resources management and hydrological modelling. *J. Hydrol.: Regional Studies* **31**, 100728 (2020).

23. Ault, T. R., Cole, J. E., Overpeck, J. T., Pederson, G. T. & Meko, D. M. Assessing the risk of persistent drought using climate model simulations and paleoclimate data. *J. Clim.* **27**, 7529–7549 (2014).

24. Flack, A. L., Kiem, A. S., Vance, T. R., Tozer, C. R. & Roberts, J. L. Comparison of published palaeoclimate records suitable for reconstructing annual to sub-decadal hydroclimatic variability in eastern Australia: implications for water resource management and planning. *Hydrol. Earth Syst. Sci.* **24**, 5699–5712 (2020).

25. Vance, T. R., van Ommen, T. D., Curran, M. A. J., Plummer, C. T. & Moy, A. D. A millennial proxy record of ENSO and Eastern Australian rainfall from the law dome ice core, East Antarctica. *J. Clim.* **26**, 710–725 (2013).

26. McMorrow, A., Van Ommen, T. D., Morgan, V. & Curran, M. A. J. Ultra-high-resolution seasonality of trace-ion species and oxygen isotope ratios in Antarctic firn over four annual cycles. *Annal. Glaciol.* **39**, 34–40 (2004).

27. Roberts, J. et al. A 2000-year annual record of snow accumulation rates for Law Dome, East Antarctica. *Clim. Past* **11**, 697–707 (2015).

28. Turner, J. et al. The dominant role of extreme precipitation events in antarctic snowfall variability. *Geophys. Res. Lett.* **46**, 3502–3511 (2019).

29. Souney, J. M. et al. A 700-year record of atmospheric circulation developed from the Law Dome ice core, East Antarctica. *J. Geophys. Res.: Atmos.* **107**, ACL 1-1–ACL 1-9 (2002).

30. Barr, C. et al. Holocene El Niño–Southern oscillation variability reflected in subtropical Australian precipitation. *Sci. Rep.* **9**, 1627 (2019).

31. Tozer, C. R. et al. An ice core derived 1013-year catchment-scale annual rainfall reconstruction in subtropical eastern Australia. *Hydrol. Earth Syst. Sci.* **20**, 1703–1717 (2016).

32. Tozer, C. R. et al. Reconstructing pre-instrumental streamflow in Eastern Australia using a water balance approach. *J. Hydrol.* **558**, 632–646 (2018).

33. Udy, D. G., Vance, T. R., Kiem, A. S., Holbrook, N. J. & Curran, M. A. J. Links between large-scale modes of climate variability and synoptic weather patterns in the Southern Indian Ocean. *J. Clim.* **34**, 883–899 (2021).

34. Risbey, J. S., Pook, M. J., McIntosh, P. C., Wheeler, M. C. & Hendon, H. H. On the remote drivers of rainfall variability in Australia. *Monthly Weather Rev.* **137**, 3233–3253 (2009).

35. McPhaden, M. J., Zebiak, S. E. & Glantz, M. H. ENSO as an integrating concept in earth science. *Science* **314**, 1740–1745 (2006).

36. Marshall, G. J. Trends in the southern annular mode from observations and reanalyses. *J. Clim.* **16**, 4134–4143 (2003).

37. Saji, N. H., Goswami, B. N., Vinayachandran, P. N. & Yamagata, T. A dipole mode in the tropical Indian Ocean. *Nature* **401**, 360–363 (1999).

38. Black, M. T. & Lane, T. P. An improved diagnostic for summertime rainfall along the eastern seaboard of Australia. *Int. J. Climatol.* **35**, 4480–4492 (2015).

39. Freund, M., Henley, B. J., Karoly, D. J., Allen, K. J. & Baker, P. J. Multi-century cool- and warm-season rainfall reconstructions for Australia's major climatic regions. *Clim. Past* **13**, 1751–1770 (2017).

40. Rakich, C. S., Holbrook, N. J. & Timbal, B. A pressure gradient metric capturing planetary-scale influences on eastern Australian rainfall. *Geophys. Res. Lett.* **35**, https://doi.org/10.1029/2007gl032970 (2008).

41. Speer, M. S., Leslie, L. M. & Fierro, A. O. Australian east coast rainfall decline related to large scale climate drivers. *Clim. Dyn.* **36**, 1419–1429 (2009).

42. Taschetto, A. S. & England, M. H. An analysis of late twentieth century trends in Australian rainfall. *Int. J. Climatol.* **29**, 791–807 (2009).

43. Holgate, C. M., Van Dijk, A. I. J. M., Evans, J. P. & Pitman, A. J. Local and remote drivers of southeast Australian drought. *Geophys. Res. Lett.* **47**, e2020GL090238 (2020).

44. Troup, A. J. The 'southern oscillation'. *Quarterly J. Royal Meteor. Soc.* **91**, 490–506 (1965).

45. Marshall, G. J., Thompson, D. W. J. & van den Broeke, M. R. The signature of southern hemisphere atmospheric circulation patterns in Antarctic precipitation. *Geophys. Res. Lett.* **44**, 11580–11589 (2017).

46. Wille, J. D. et al. Antarctic atmospheric river climatology and precipitation impacts. *J. Geophys. Res.: Atmos.* **126**, e2020JD033788 (2021).

47. Lim, E.-P. et al. Australian hot and dry extremes induced by weakenings of the stratospheric polar vortex. *Nat. Geosci.* **12**, 896–901 (2019).

48. Scarchilli, C., Frezzotti, M. & Ruti, P. M. Snow precipitation at four ice core sites in East Antarctica: provenance, seasonality and blocking factors. *Clim. Dyn.* **37**, 2107–2125 (2011).

49. Crockart, C. K. et al. El Niño–Southern oscillation signal in a new East Antarctic ice core, Mount Brown South. *Clim. Past* **17**, 1795–1818 (2021).

50. Kiem, A. S., Franks, S. W. & Kuczera, G. Multi-decadal variability of flood risk. *Geophys. Res. Lett.* **30**, https://doi.org/10.1029/2002gl015992 (2003).

51. Abram, N. J. et al. Connections of climate change and variability to large and extreme forest fires in southeast Australia. *Commun. Earth Environ.* **2**, 8 (2021).

52. Yu, J.-Y. & Kim, S. T. Identifying the types of major El Niño events since 1870. *Int. J. Climatol.* **33**, 2105–2112 (2013).

53. Freund, M. B., Marshall, A. G., Wheeler, M. C. & Brown, J. N. Central Pacific El Niño as a precursor to summer drought-breaking rainfall over southeastern Australia. *Geophys. Res. Lett.* **48**, e2020GL091131 (2021).

54. Lee, T. et al. Record warming in the South Pacific and western Antarctica associated with the strong central-Pacific El Niño in 2009–10. *Geophys. Res. Lett.* **37**, https://doi.org/10.1029/2010GL044865 (2010).

55. Jong, L. M. et al. 2000 years of annual ice core data from Law Dome, East Antarctica. *Earth Syst. Sci. Data Discuss.* **2022**, 1–26 (2022).

56. Vance, T. R. et al. Optimal site selection for a high-resolution ice core record in East Antarctica. *Clim. Past* **12**, 595–610 (2016).

57. Udy, D., Vance, T. R., Kiem, A., Holbrook, N. & Curran, M. Daily synoptic weather types of southern Indian Ocean: January 1979-October 2018. Australian Antarctic Data Centre. https://doi.org/10.4225/15/58eedf00d78fe (2020).

58. Dee, D. P. et al. The ERA-Interim reanalysis: configuration and performance of the data assimilation system. *Quarterly J. Royal Meteorol. Soc.* **137**, 553–597 (2011).

59. Jiang, N., Cheung, K., Luo, K., Beggs, P. J. & Zhou, W. On two different objective procedures for classifying synoptic weather types over east Australia. *Int. J. Climatol.* **32**, 1475–1494 (2012).

60. Hewitson, B. C. & Crane, R. G. Self-organizing maps: applications to synoptic climatology. *Clim. Res.* **22**, 13–26 (2002).

61. Hope, P. K., Drosdowsky, W. & Nicholls, N. Shifts in the synoptic systems influencing southwest Western Australia. *Clim. Dyn.* **26**, 751–764 (2006).

62. Reusch, D. B., Hewitson, B. C. & Alley, R. B. Towards ice-core-based synoptic reconstructions of west antarctic climate with artificial neural networks. *Int. J. Climatol.* **25**, 581–610 (2005).

63. Trenberth, K. The climate data guide: Nino SST indices (Nino1+2,3,3.4,4; ONI and TNI), https://climatedataguide.ucar.edu/climate-data/nino-sst-indices-nino-12-3-34-4-oni-and-tni (2020).

64. Erickson, D. J., Merrill, J. T. & Duce, R. A. Seasonal estimates of global atmospheric sea-salt distributions. *J. Geophys. Res.: Atmos.* **91**, 1067–1072 (1986).

65. Australian Bureau of Meteorology. Australian Gridded Climate Data (AGCD)/AWAP v1.0.0 Snapshot (1900-01-01 to 2018-12-31). https://doi.org/10.4227/166/5a8647d1c23e0 (2019).

66. Curran, M. et al. The Law Dome ice core 2000 year dataset collection. *Australian Antarctic Data Centre* https://doi.org/10.26179/5zm0-v192 (2021).

67. Masson-Delmotte, V. et al. Recent southern Indian Ocean climate variability inferred from a Law Dome ice core: new insights for the interpretation of coastal Antarctic isotopic records. *Clim. Dyn.* **21**, 153–166 (2003).

68. van Ommen, T. D. & Morgan, V. Snowfall increase in coastal East Antarctica linked with southwest Western Australian drought. *Nat. Geosci.* **3**, 267, https://www.nature.com/articles/ngeo761-supplementary-information (2010).

69. van Ommen, T. D. & Morgan, V. Calibrating the ice core paleothermometer using seasonality. *J. Geophys. Res.: Atmos.* **102**, 9351–9357 (1997).

70. Plummer, C. T. et al. An independently dated 2000-yr volcanic record from Law Dome, East Antarctica, including a new perspective on the dating of the 1450s CE eruption of Kuwae, Vanuatu. *Clim. Past* **8**, 1929–1940 (2012).

71. Benassai, S. et al. Sea-spray deposition in Antarctic coastal and plateau areas from ITASE traverses. *Annal. Glaciol.* **41**, 32–40 (2005).

72. Morgan, V. I. et al. Site information and initial results from deep ice drilling on Law Dome, Antarctica. *J. Glaciol.* **43**, 3–10 (1997).

Acknowledgements

Author contributions

D.U. led and designed the study, undertaking the majority of the data analysis, interpretation and writing of the manuscript. T.V. and A.K. conceived and designed the study. T.V., A.K. and N.H. contributed substantially to the data interpretation and critically revising of the manuscript.

Competing interests

The authors declare no competing interests.

Additional information

Supplementary information The online version contains supplementary material available at https://doi.org/10.1038/s43247-022-00502-w.

Correspondence and requests for materials should be addressed to Danielle G. Udy.

Peer review information *Communications Earth & Environment* thanks the anonymous reviewers for their contribution to the peer review of this work. Primary Handling Editors: Clara Orbe, Joe Aslin, Heike Langenberg.

Reprints and permission information is available at http://www.nature.com/reprints

Publisher's note Springer Nature remains neutral with regard to jurisdictional claims in published maps and institutional affiliations.